PCCP

COMMUNICATION

View Article Online
View Journal | View Issue

Cite this: *Phys. Chem. Chem. Phys.*, 2021, **23**, 15480

Received 7th April 2021,
Accepted 6th July 2021

DOI: 10.1039/d1cp01498f

rsc.li/pccp

Silver oxide model surface improves computational simulation of surface-enhanced Raman spectroscopy on silver nanoparticles†

Scott G. Harroun, *[a] Yaoting Zhang,[b] Tzu-Heng Chen, [cd] Huan-Tsung Chang *[c] and Alexis Vallée-Bélisle *[ae]

Surface-enhanced Raman spectroscopy (SERS) coupled with density functional theory (DFT) computations can characterise the adsorption orientation of a molecule on a nanoparticle surface. When using DFT to simulate SERS on a silver surface, one typically employs an atom (Ag), ion (Ag^+), or cluster (Ag_x or Ag_x^+) as the model surface. Here, by examining the nucleobase 2,6-diaminopurine (2,6-DAP) and then generalising our strategy to three other molecules, we show that employing silver oxide (Ag_2O) as the model surface can quantitatively improve the accuracy of simulated SERS.

Surface-enhanced Raman spectroscopy (SERS) is the large enhancement of the Raman spectrum of a molecule adsorbed on metal nanoparticles.[1] Its applications range from detection and analysis of biomolecules and microorganisms to characterisation of materials.[2–5] Although various metals can be employed for SERS, gold and silver are the most popular.[6] With silver nanoparticles (Ag NPs), it is well known that their exposure to air can result in the formation of silver oxide (Ag_2O), which can affect their plasmonic properties.[7,8] While some recent SERS studies have used intentionally oxidised Ag nanomaterials,[9,10] unintentional oxidation is typically seen as detrimental because it reduces the SERS enhancement factor.[11–15] Although specialised techniques to avoid oxidation do exist,[16–20] many SERS researchers simply use their Ag NPs as quickly as possible after synthesis.[15] While some attenuation of the overall signal intensity is tolerable, the presence of Ag_2O on Ag NPs could also subtly affect the shape of the SERS spectrum.[12,19,21] However, this has not been considered in previous simulations of SERS on silver surfaces.

Rather than attempting to deduce a molecule's adsorption orientation by comparing normal Raman and SERS *via* the surface selection rules,[22] one can employ density functional theory (DFT) quantum mechanical computations to elucidate its surface-adsorbed state.[23] Using this approach, one first performs computations for the molecule of interest interacting with a model surface in all possible (or reasonable) adsorption orientations. This involves geometrical optimisation followed by simulation of spectra. Then, the correct structure is often the one whose simulated spectrum is most similar to the experimental spectrum; it also usually has the lowest energy.[23] For silver, the model surface can be a single atom (Ag) or ion (Ag^+),[24–26] or a larger cluster (Ag_x or Ag_x^+, where x is the number of atoms, typically 2–20).[26–33] Interestingly, several studies involving silver have reported better simulations with positively charged model surfaces.[24,25,27] Nevertheless, since simulations of SERS can display errors (*e.g.*, inaccurate wavenumbers or intensities), it remains imperative to develop new and creative strategies.[34–36] Indeed, prominent members of the SERS community recently identified improving simulations as important for the advancement of SERS.[1] With this in mind, here we explored Ag_2O as a model surface to simulate SERS on Ag NPs. To the best of our knowledge, this approach has never been tried in previous studies with silver nanomaterials.[37]

We selected 2,6-diaminopurine (2,6-DAP), also called 2-aminoadenine, as a model analyte. Natural genomic occurrence of 2,6-DAP was once thought to be rare.[38,39] In one case, it was detected on a meteorite, and determined unlikely to be from terrestrial contamination, but instead, of extra-terrestrial origin.[40] However, a series of recent studies has brought renewed attention to genomic 2,6-DAP in bacteriophage viruses.[41–45] Other recent works have proposed 2,6-DAP as a candidate drug for the treatment of genetic diseases caused by nonsense mutations,[46] as well as its possible role in the repair of DNA lesions under prebiotic conditions.[47] Elsewhere, Au NPs functionalised with 2,6-DAP displayed catalytic properties.[48] Thus, characterising its interaction

[a] *Laboratory of Biosensors & Nanomachines, Département de Chimie, Université de Montréal, Montréal, QC, H3C 3J7, Canada. E-mail: sg.harroun@umontreal.ca, a.vallee-belisle@umontreal.ca*
[b] *Department of Chemistry, Queen's University, Kingston, ON, K7L 3N6, Canada*
[c] *Department of Chemistry, National Taiwan University, Taipei, 10617, Taiwan. E-mail: changht@ntu.edu.tw*
[d] *Laboratory of Nanoscale Biology, Institute of Bioengineering, School of Engineering, École Polytechnique Fédérale de Lausanne (EPFL), Lausanne 1015, Switzerland*
[e] *Département de Biochimie et Médicine Moléculaire, Université de Montréal, Montréal, QC, H3C 3J7, Canada*

† Electronic supplementary information (ESI) available: Materials and methods, supplementary figures, and tables. See DOI: 10.1039/d1cp01498f

with the surface of metal NPs could help future analytical, biomedical, genomic and catalytic studies.

We first recorded the normal Raman spectrum of 2,6-DAP in the solid phase. We also simulated its Raman spectrum *in vacuo* by DFT, which was found to be in good agreement (*n.b.*, B3LYP functional with the 6-311+G(2d,p) (C, N, O, H) and LanL2DZ (Ag) basis sets). See Fig. S1, ESI† for Raman spectra and Tables S1 and S2, ESI† for vibrational assignments. Next, we prepared Ag NPs for SERS by reduction of $AgNO_3$ with citrate. We characterised them by ultraviolet-visible spectroscopy (UV-Vis), scanning electron microscopy (SEM), Raman spectroscopy, and X-ray photoelectron spectroscopy (XPS). Our Ag NPs were comparable to those used in other SERS studies (Fig. S2, ESI†). We then recorded the SERS spectrum of 2,6-DAP adsorbed on the Ag NPs. The shift of the ring breathing band of 2,6-DAP from 637 cm^{-1} in Raman to 650 cm^{-1} in SERS, as well as its relative enhancement in SERS, suggests a vertical adsorption orientation with respect to the ring plane of 2,6-DAP (Fig. S3, ESI†).[22,49] However, this does not provide detailed information about which side of the molecule interacts with the Ag NPs. To obtain more information about 2,6-DAP on the surface, we performed computations of one Ag^+ ion interacting with each nitrogen atom of 2,6-DAP.[24,25] The geometrical optimisation step gave seven stable complexes, named Ag^+/2,6-DAP-i to -vii (Fig. 1A and see Table S3, ESI† for relative energies and Boltzmann distribution, and Table S4, ESI† for Ag–N bond lengths). Next, we simulated SERS for each complex (Fig. 1B). Among these, the most accurate simulated spectrum was obtained with the lowest energy complex, Ag^+/2,6-DAP-i. For example, its ring breathing band is simulated at 650 cm^{-1}, whereas for all of the others, this band is inaccurately simulated between 621 cm^{-1} to 634 cm^{-1}. However, despite Ag^+/2,6-DAP-i being the most stable and having the most accurate spectrum among these, this simulation remains unsatisfactory.

We therefore explored other silver model surfaces with the same configuration as the Ag^+/2,6-DAP-i complex to see if they could improve the accuracy of the simulation. These model surfaces were Ag, Ag_4^+ and Ag_4,[24–29] which gave the complexes Ag/2,6-DAP-i, Ag_4^+/2,6-DAP-i, and Ag_4/2,6-DAP-i, respectively. For the first time, we also used Ag_2O as a model surface, which gave Ag_2O/2,6-DAP-i (Fig. 2A). We simulated the SERS spectra for these complexes and then compared them with the experimental SERS of 2,6-DAP on Ag NPs (Fig. 2B).

We quantitatively compared the experimental spectrum *versus* the five simulated spectra in terms of their band wavenumber and relative intensity (Table S5, ESI†). We first considered ten bands of 2,6-DAP that were present in all of the spectra and then determined their mean absolute error (MAE) relative to the experimental spectrum. The simulated spectra ranked from least to most accurate are Ag^+/2,6-DAP-i, Ag/2,6-DAP-i, Ag_4^+/2,6-DAP-i, Ag_4/2,6-DAP-i, and Ag_2O/2,6-DAP-i. Thus, for wavenumber and relative intensity, Ag_2O/2,6-DAP-i provides the most accurate simulation.

To further assess the quality of the simulations, we examined their spectral differences that are not quantifiable in a systematic manner, such as erroneous bands present in some simulated

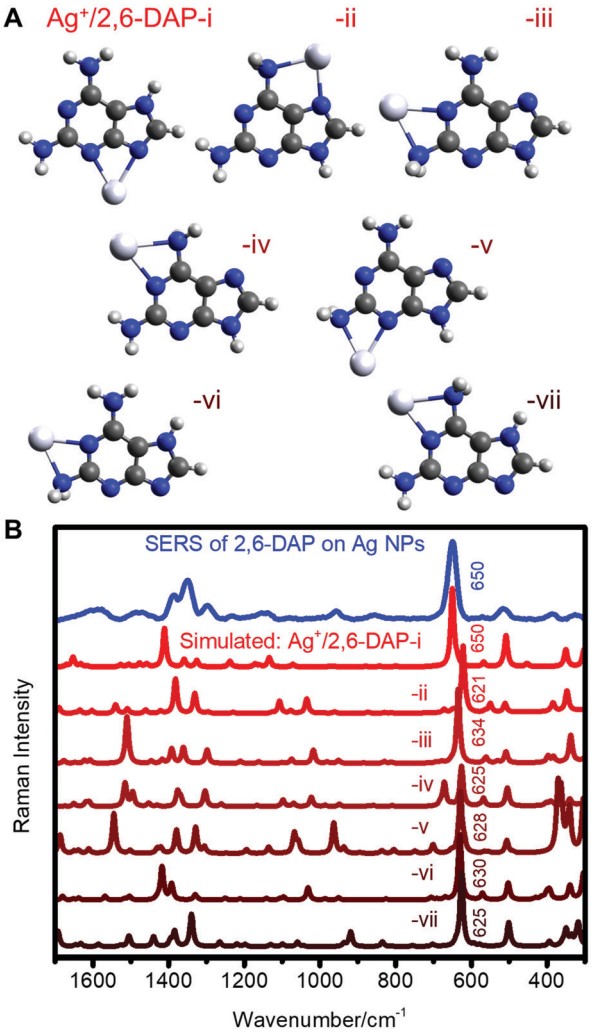

Fig. 1 (A) Stable Ag^+/2,6-DAP complexes obtained using DFT ranked from the lowest (i) to the highest (vii) energy. (B) Experimental SERS spectrum of 2,6-DAP and simulated spectra of the different Ag^+/2,6-DAP complexes. Atomic colour scheme: blue = N, grey = C, white = H, silver = Ag.

spectra but not all of them. For example, the two erroneous amino twisting bands of Ag/2,6-DAP-i and Ag_4/2,6-DAP-i at 486 cm^{-1} and 437 cm^{-1}, respectively, are not observed in the experimental SERS spectrum (Fig. 2 and 3A). This is not surprising and reflects well the limitations and challenges of simulating SERS, as these model surfaces may not represent the exact surface interface. In comparison, the two obvious erroneous bands observed in the Ag_2O/2,6-DAP-i spectrum at 487 cm^{-1} and 550 cm^{-1} are mainly due to Ag_2O stretching rather than the 2,6-DAP component (Fig. 2 and 3B). Note that a band near 490 cm^{-1} is observed in the Raman spectrum of pure Ag_2O,[50] but typically will not be present in the spectrum of Ag NPs except after severe oxidative treatment with ozone.[12] Furthermore, the intense band near 550 cm^{-1} is experimentally infrared-active but Raman-inactive.[50] Thus, as expected, we also did not observe them in the spectrum of our Ag NPs without 2,6-DAP (Fig. S2C, ESI†). The presence of these bands in the simulated spectrum of Ag_2O/2,6-DAP-i, however, is attributed to

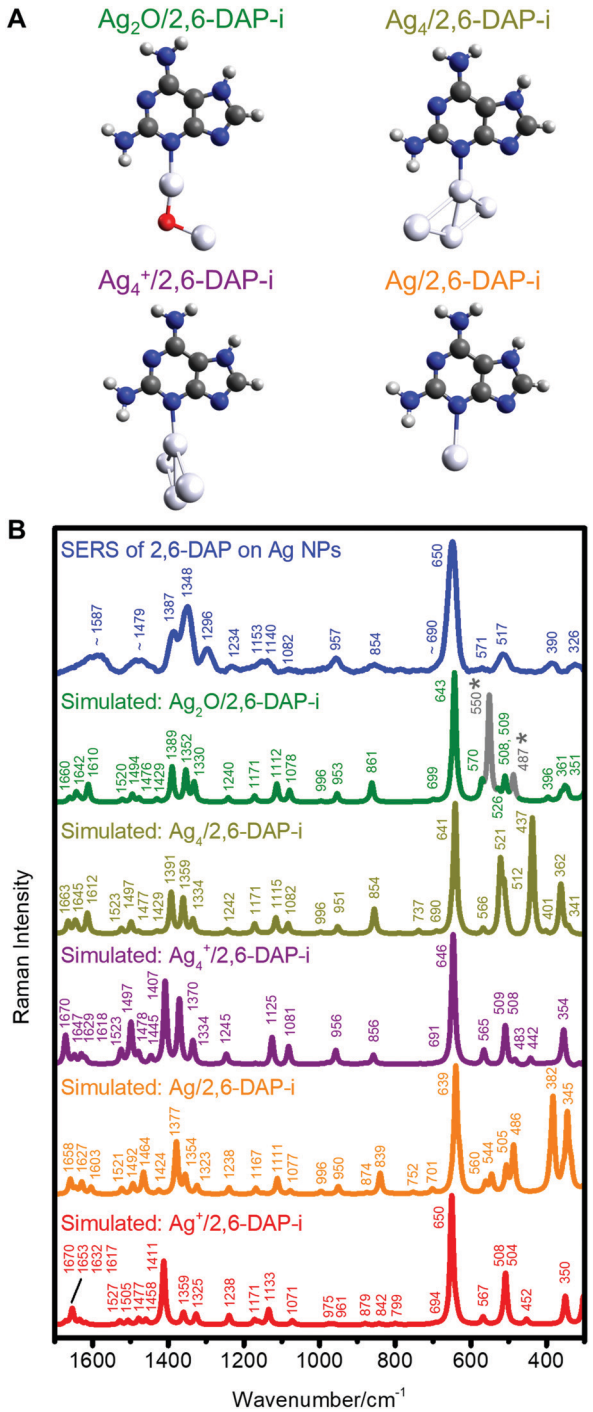

Fig. 2 (A) DFT simulation of 2,6-DAP using various silver model surfaces. (B) Experimental SERS spectrum of 2,6-DAP and simulated SERS spectra of Ag_2O/2,6-DAP-i, Ag_4/2,6-DAP-i, Ag_4^+/2,6-DAP-i, Ag/2,6-DAP-i and Ag^+/2,6-DAP-i. The most predictive simulation is provided by Ag_2O/2,6-DAP-i. Note also that Ag_2O stretching vibrations are indicated with an asterisk (*). Atomic colour scheme: blue = N, grey = C, red = O, white = H, silver = Ag. See Fig. S4 and S5, ESI† for averaging and baseline correction. All spectra are normalised relative to the most intense band.

its simplification relative to the real surface of the Ag NPs. The Ag_2O model surface is unrestrained in our simulation, but in the experimental system the Ag_2O vibrations might be much

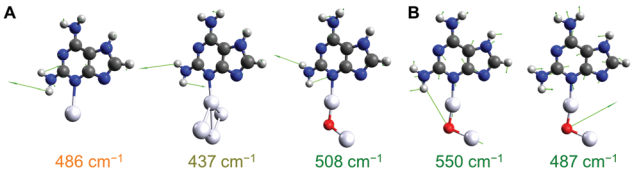

Fig. 3 Visualisation of selected modes of vibration: (A) amino twisting for Ag/2,6-DAP-i, Ag_4/2,6-DAP-i and Ag_2O/2,6-DAP-i, as well as (B) asymmetric and symmetric Ag_2O stretching for Ag_2O/2,6-DAP-i.

less prominent because of the crystal-like structure. These bands in the simulation also do not arise due to a change of symmetry *via* the presence of 2,6-DAP, since a similar error occurs in a system with only Ag_2O and no ligand (Fig. S6, ESI†). Computationally expensive plane-wave DFT incorporating periodic boundary conditions might correctly compute these Raman bands.[51,52] Nevertheless, from a practical perspective, they simply will not appear in experimental SERS; they are an artifact of the simulation. Therefore, we propose that if these two Ag_2O stretching bands, and only these, are omitted from consideration as artifacts of the simulation, then Ag_2O/2,6-DAP-i provides the most accurate result. For ways to omit these bands, see Fig. S7, ESI.†

We next explored the origin of why some complexes provide a better simulation of SERS than others. For Ag^+/2,6-DAP-i, which provides the worst simulation, it likely has a geometry that does not represent the experimental system, as this bidentate complex has two Ag–N bonds (2.369 Å and 2.478 Å; Table S4, ESI†). Indeed, all of the others have monodentate interaction with the model surface. For Ag/2,6-DAP-i, the calculated Ag–N bond length is quite weak (2.529 Å). This length is not impossible for Ag–N bonds, but greater than the typical bond length of about 2.1 to 2.4 Å.[53–55] Conversely, for Ag_4^+/2,6-DAP-i, Ag_4/2,6-DAP-i and Ag_2O/2,6-DAP-i, the Ag–N bond lengths are in the expected range (2.218 Å, 2.273 Å, and 2.163 Å, respectively). Thus, bond length, coordination, and model surface type contribute to a better simulation of SERS.

To test the potential generality of this method, we explored whether Ag_2O can work as a model surface for simulation of SERS of other molecules adsorbed on Ag nanomaterials. We selected three molecules for which good SERS simulations have been reported: adenine, melamine, and 4,4′-bipyridine (4,4′-bpy).[26–28] We then compared the results of those studies with our own simulations that employed Ag_2O as a model surface. Necessarily, the molecule was bound to Ag_2O at the same site as reported elsewhere (Fig. S8A, ESI†).

Adenine has been extensively characterised with SERS.[56] The most accurate simulation was achieved by Huang *et al.* with a Ag_4^+/adenine complex,[27] which we compared with our Ag_2O/adenine (Fig. S8B and Table S6, ESI†). Although both provide great simulations, the mean absolute error (MAE) value is somewhat lower with Ag_2O/adenine. Moreover, the most intense band near 732 cm^{-1} is more accurately simulated by Ag_2O/adenine at 736 cm^{-1} compared to Ag_4^+/adenine at 721 cm^{-1}. Next, we considered melamine (Fig. S8B and Table S7, ESI†). An *et al.* simulated SERS of melamine by various

Ag_x/melamine complexes, with Ag_4/melamine providing the best result.[28] Ag_4/melamine and Ag_2O/melamine have similar accuracy for band wavenumber, although Ag_4/melamine has a somewhat lower MAE value. Notably, however, Ag_2O/melamine displays better relative band intensities. Finally, we considered 4,4′-bpy (Fig. S8B and Table S8, ESI†). Zhuang *et al.* simulated SERS using Ag/4,4′-bpy, Ag_3/4,4′-bpy and Ag_4/4,4′-bpy complexes.[26] For this, Ag_3/4,4′-bpy and Ag_2O/4,4′-bpy are better for wavenumber, as determined by MAE, but Ag/4,4′-bpy and Ag_4/4,4′-bpy are better for relative intensities. Overall, this comparison with other studies[26–28] reveals that Ag_2O performs as well as, and in some cases better than, the standard model surfaces used to simulate SERS.

Here, we have shown that one can employ Ag_2O as a model surface for simulation of SERS on Ag NPs. We propose that this method can improve simulations relative to those obtained by silver atoms, ions, or clusters. We first focussed on the nucleobase 2,6-DAP, and then generalised our strategy to three other molecules. We demonstrated the benefits of our strategy by quantitative comparison of experimental and simulated band wavenumbers and relative intensities, as well as by careful examination of the bands in the various spectra. This computational approach remains imperfect, however, which reflects the great challenge of accurately simulating SERS.[1] Therefore, our findings reported herein add another efficient option to the toolbox for this important task. Further experimental and theoretical investigations remain pertinent in order to push the limits of combining SERS and DFT.

We conclude by considering that the SERS signal arises due to a metal/adsorbate complex wherein the electronic structure of not only the adsorbate is modified, but also for some nearby metal atoms.[57] Thus, speculatively, it might be possible to couple SERS with DFT calculations in order to characterise not only a molecule's adsorption orientation, but also its specific adsorption site.[58,59] One could compare model surfaces that have different charges or sizes, as well as with or without oxidation. Additionally, our findings could be important for applications such as catalysis,[60–62] the study of molecules on metal and metal oxide surfaces,[63] and SERS-based screening of modified DNA.[2]

Conflicts of interest

There are no conflicts of interest to declare.

Acknowledgements

S. G. H. acknowledges doctoral funding from the Natural Sciences and Engineering Research Council of Canada (NSERC) and the Fonds de Recherché du Québec – Nature et Technologies (FRQNT). Y. Z. acknowledges ACEnet (Canada) for computational resources. A. V. B. is a Canada Research Chair in Bioengineering and Bionanotechnology, Tier II. C. A. Villeneuve (UdeM) is acknowledged for helpful comments on the manuscript.

Notes and references

1 J. Langer, D. Jimenez de Aberasturi, J. Aizpurua, R. A. Alvarez-Puebla, B. Auguié, J. J. Baumberg, G. C. Bazan, S. E. J. Bell, A. Boisen, A. G. Brolo, J. Choo, D. Cialla-May, V. Deckert, L. Fabris, K. Faulds, F. J. García de Abajo, R. Goodacre, D. Graham, A. J. Haes, C. L. Haynes, C. Huck, T. Itoh, M. Käll, J. Kneipp, N. A. Kotov, H. Kuang, E. C. Le Ru, H. K. Lee, J.-F. Li, X. Y. Ling, S. A. Maier, T. Mayerhöfer, M. Moskovits, K. Murakoshi, J.-M. Nam, S. Nie, Y. Ozaki, I. Pastoriza-Santos, J. Perez-Juste, J. Popp, A. Pucci, S. Reich, B. Ren, G. C. Schatz, T. Shegai, S. Schlücker, L.-L. Tay, K. G. Thomas, Z.-Q. Tian, R. P. Van Duyne, T. Vo-Dinh, Y. Wang, K. A. Willets, C. Xu, H. Xu, Y. Xu, Y. S. Yamamoto, B. Zhao and L. M. Liz-Marzán, *ACS Nano*, 2020, **14**, 28–117.
2 J. Morla-Folch, H.-n. Xie, P. Gisbert-Quilis, S. G.-d. Pedro, N. Pazos-Perez, R. A. Alvarez-Puebla and L. Guerrini, *Angew. Chem., Int. Ed.*, 2015, **54**, 13650–13654.
3 M. Perez-Estebanez, S. Hernandez, J. V. Perales-Rondon, E. Gomez, A. Heras and A. Colina, *Electrochim. Acta*, 2020, **353**, 136560.
4 T. Lemma, J. Wang, K. Arstila, V. P. Hytönen and J. J. Toppari, *Spectrochim. Acta, Part A*, 2019, **218**, 299–307.
5 M. Muniz-Miranda, F. Muniz-Miranda, S. Caporali, N. Calisi and A. Pedone, *Appl. Surf. Sci.*, 2018, **457**, 98–103.
6 R. D. Rodriguez, E. Sheremet, M. Nesterov, S. Moras, M. Rahaman, T. Weiss, M. Hietschold and D. R. T. Zahn, *Sens. Actuators, B*, 2018, **262**, 922–927.
7 Y. Yin, Z.-Y. Li, Z. Zhong, B. Gates, Y. Xia and S. Venkateswaran, *J. Mater. Chem.*, 2002, **12**, 522–527.
8 A. Henglein, *Chem. Mater.*, 1998, **10**, 444–450.
9 H.-L. Chen, Z.-H. Yang and S. Lee, *Langmuir*, 2016, **32**, 10184–10188.
10 C. Tan, Z. Zhang, Y. Qu and L. He, *Langmuir*, 2017, **33**, 5345–5352.
11 M. Erol, Y. Han, S. K. Stanley, C. M. Stafford, H. Du and S. Sukhishvili, *J. Am. Chem. Soc.*, 2009, **131**, 7480–7481.
12 Y. Han, R. Lupitskyy, T.-M. Chou, C. M. Stafford, H. Du and S. Sukhishvili, *Anal. Chem.*, 2011, **83**, 5873–5880.
13 H. Qi, D. Alexson, O. Glembocki and S. M. Prokes, *Nanotechnology*, 2010, **21**, 215706.
14 Z.-H. Yang, C.-H. Ho and S. Lee, *Appl. Surf. Sci.*, 2015, **349**, 609–614.
15 A. Matikainen, T. Nuutinen, T. Itkonen, S. Heinilehto, J. Puustinen, J. Hiltunen, J. Lappalainen, P. Karioja and P. Vahimaa, *Sci. Rep.*, 2016, **6**, 37192.
16 X. Li, J. Li, X. Zhou, Y. Ma, Z. Zheng, X. Duan and Y. Qu, *Carbon*, 2014, **66**, 713–719.
17 L. Maria, B. Iris, D. Babak, K. Tong-Ho, G. M. M., J. Wenyuan, B. G. V., B. A. S., H. Kurt and B. Giovanni, *Adv. Funct. Mater.*, 2014, **24**, 1864–1878.
18 C. Liu, X. Xu, W. Hu, X. Yang, P. Zhou, G. Qiu, W. Ye, Y. Li and C. Jiang, *Anal. Chem.*, 2018, **90**, 9805–9812.
19 C. Ma, M. J. Trujillo and J. P. Camden, *ACS Appl. Mater. Interfaces*, 2016, **8**, 23978–23984.
20 Y. Liu, H. Wu, L. Ma, S. Zou, Y. Ling and Z. Zhang, *Nanoscale*, 2018, **10**, 19863–19870.

21 T. Chen, A. Pal, J. Gao, Y. Han, H. Chen, S. Sukhishvili, H. Du and S. G. Podkolzin, *J. Phys. Chem. C*, 2015, **119**, 24475–24488.
22 X. Gao, J. P. Davies and M. J. Weaver, *J. Phys. Chem.*, 1990, **94**, 6858–6864.
23 M. Muniz-Miranda, F. Muniz-Miranda and A. Pedone, in *Metal Nanoparticles and Clusters: advances in Synthesis, Properties and Applications*, ed. F. L. Deepak, Springer International Publishing, Cham, 2018, pp. 55–87, DOI: 10.1007/978-3-319-68053-8_3.
24 M.-E. Yu, B.-S. Cheong and H.-G. Cho, *Bull. Korean Chem. Soc.*, 2017, **38**, 928–934.
25 M. Pagliai, S. Caporali, M. Muniz-Miranda, G. Pratesi and V. Schettino, *J. Phys. Chem. Lett.*, 2012, **3**, 242–245.
26 Z. Zhuang, W. Ruan, N. Ji, X. Shang, X. Wang and B. Zhao, *Vib. Spectrosc.*, 2009, **49**, 118–123.
27 R. Huang, H.-T. Yang, L. Cui, D.-Y. Wu, B. Ren and Z.-Q. Tian, *J. Phys. Chem. C*, 2013, **117**, 23730–23737.
28 N. T. T. An, D. Q. Dao, P. C. Nam, B. T. Huy and H. Nhung Tran, *Spectrochim. Acta, Part A*, 2016, **169**, 230–237.
29 M. Kamran, M. Haroon, S. A. Popoola, A. R. Almohammedi, A. A. Al-Saadi and T. A. Saleh, *J. Mol. Liq.*, 2019, **273**, 536–542.
30 M. Sun, S. Wan, Y. Liu, Y. Jia and H. Xu, *J. Raman Spectrosc.*, 2008, **39**, 402–408.
31 M. Sun, S. Zhang, Y. Fang, Z. Yang, D. Wu, B. Dong and H. Xu, *J. Phys. Chem. C*, 2009, **113**, 19328–19334.
32 M. Sun, Y. Fang, Z. Yang and H. Xu, *Phys. Chem. Chem. Phys.*, 2009, **11**, 9412–9419.
33 M. Muniz-Miranda, F. Muniz-Miranda and A. Pedone, *Phys. Chem. Chem. Phys.*, 2016, **18**, 5974–5980.
34 W. Hu, S. Ye, Y. Zhang, T. Li, G. Zhang, Y. Luo, S. Mukamel and J. Jiang, *J. Phys. Chem. Lett.*, 2019, **10**, 6026–6031.
35 L. M. Freeman, A. Smolyaninov, L. Pang and Y. Fainman, *Sci. Rep.*, 2016, **6**, 23535.
36 J. M. Hermida-Ramon, L. Guerrini and R. A. Alvarez-Puebla, *J. Phys. Chem. A*, 2013, **117**, 4584–4590.
37 L. Jiang, T. You, P. Yin, Y. Shang, D. Zhang, L. Guo and S. Yang, *Nanoscale*, 2013, **5**, 2784–2789.
38 M. Kirnos, I. Y. Khudyakov, N. Alexandrushkina and B. Vanyushin, *Nature*, 1977, **270**, 369.
39 I. Y. Khudyakov, M. D. Kirnos, N. I. Alexandrushkina and B. F. Vanyushin, *Virology*, 1978, **88**, 8–18.
40 M. P. Callahan, K. E. Smith, H. J. Cleaves, J. Ruzicka, J. C. Stern, D. P. Glavin, C. H. House and J. P. Dworkin, *Proc. Natl. Acad. Sci. U. S. A.*, 2011, **108**, 13995–13998.
41 M. W. Grome and F. J. Isaacs, *Science*, 2021, **372**, 460–461.
42 Y. Zhou, X. Xu, Y. Wei, Y. Cheng, Y. Guo, I. Khudyakov, F. Liu, P. He, Z. Song, Z. Li, Y. Gao, E. L. Ang, H. Zhao, Y. Zhang and S. Zhao, *Science*, 2021, **372**, 512–516.
43 D. Sleiman, P. S. Garcia, M. Lagune, J. Loc'h, A. Haouz, N. Taib, P. Röthlisberger, S. Gribaldo, P. Marlière and P. A. Kaminski, *Science*, 2021, **372**, 516–520.
44 V. Pezo, F. Jaziri, P.-Y. Bourguignon, D. Louis, D. Jacobs-Sera, J. Rozenski, S. Pochet, P. Herdewijn, G. F. Hatfull, P.-A. Kaminski and P. Marliere, *Science*, 2021, **372**, 520–524.
45 D. Czernecki, P. Legrand, M. Tekpinar, S. Rosario, P.-A. Kaminski and M. Delarue, *Nat. Commun.*, 2021, **12**, 2420.
46 C. Trzaska, S. Amand, C. Bailly, C. Leroy, V. Marchand, E. Duvernois-Berthet, J.-M. Saliou, H. Benhabiles, E. Werkmeister, T. Chassat, R. Guilbert, D. Hannebique, A. Mouray, M.-C. Copin, P.-A. Moreau, E. Adriaenssens, A. Kulozik, E. Westhof, D. Tulasne, Y. Motorin, S. Rebuffat and F. Lejeune, *Nat. Commun.*, 2020, **11**, 1509.
47 R. Szabla, M. Zdrowowicz, P. Spisz, N. J. Green, P. Stadlbauer, H. Kruse, J. Šponer and J. Rak, *Nat. Commun.*, 2021, **12**, 3018.
48 Y. Wu, Y. Chen, Y. Li, J. Huang, H. Yu and Z. Wang, *Sens. Actuators, B*, 2018, **270**, 443–451.
49 B. Giese and D. McNaughton, *J. Phys. Chem. B*, 2002, **106**, 101–112.
50 G. I. N. Waterhouse, G. A. Bowmaker and J. B. Metson, *Phys. Chem. Chem. Phys.*, 2001, **3**, 3838–3845.
51 M. Akhtar, M. Menon, M. Sunkara, G. Sumanasekera, A. Durygin and J. B. Jasinski, *J. Alloys Compd.*, 2015, **641**, 87–92.
52 K. Galav, S. Paliwal, V. Maurya, G. Sharma and K. Joshi, *Indian J. Pure Appl. Phys.*, 2019, **57**, 918–922.
53 F. Belanger-Gariepy and A. L. Beauchamp, *J. Am. Chem. Soc.*, 1980, **102**, 3461–3464.
54 C. S. Purohit and S. Verma, *J. Am. Chem. Soc.*, 2006, **128**, 400–401.
55 R. P. Feazell, C. E. Carson and K. K. Klausmeyer, *Inorg. Chem.*, 2006, **45**, 2635–2643.
56 S. G. Harroun, *ChemPhysChem*, 2018, **19**, 1003–1015.
57 M. Moskovits, *Phys. Chem. Chem. Phys.*, 2013, **15**, 5301–5311.
58 S. Caporali, F. Muniz-Miranda, A. Pedone and M. Muniz-Miranda, *Sensors*, 2019, **19**, 2700.
59 I. Šloufová, M. Procházka and B. Vlčková, *J. Raman Spectrosc.*, 2015, **46**, 39–46.
60 C. Queffélec, F. Forato, B. Bujoli, D. A. Knight, E. Fonda and B. Humbert, *Phys. Chem. Chem. Phys.*, 2020, **22**, 2193–2199.
61 A. Kuzume, M. Ozawa, Y. Tang, Y. Yamada, N. Haruta and K. Yamamoto, *Sci. Adv.*, 2019, **5**, eaax6455.
62 H. Zhong, J. Chen, J. Chen, R. Tao, J. Jiang, Y. Hu, J. Xu, T. Zhang and J. Liao, *Phys. Chem. Chem. Phys.*, 2020, **22**, 23482–23490.
63 S. Bercha, S. Bhasker-Ranganath, X. Zheng, K. Beranová, M. Vorokhta, R. G. Acres, T. Skála, V. Matolín, K. C. Prince, Y. Xu and N. Tsud, *Appl. Surf. Sci.*, 2020, **530**, 147257.

